ARTICLES
PUBLISHED ONLINE: 12 DECEMBER 2016 | DOI: 10.1038/NGEO2848
nature geoscience

Global atmospheric teleconnections during Dansgaard–Oeschger events

Bradley R. Markle[1]*, Eric J. Steig[1,2], Christo Buizert[3], Spruce W. Schoenemann[1], Cecilia M. Bitz[2], T. J. Fudge[1], Joel B. Pedro[4], Qinghua Ding[5], Tyler R. Jones[6], James W. C. White[6] and Todd Sowers[7]

During the last glacial period, the North Atlantic region experienced a series of Dansgaard–Oeschger cycles in which climate abruptly alternated between warm and cold periods. Corresponding variations in Antarctic surface temperature were out of phase with their Northern Hemisphere counterparts. The temperature relationship between the hemispheres is commonly attributed to an interhemispheric redistribution of heat by the ocean overturning circulation. Changes in ocean heat transport should be accompanied by changes in atmospheric circulation to satisfy global energy budget constraints. Although changes in tropical atmospheric circulation linked to abrupt events in the Northern Hemisphere are well documented, evidence for predicted changes in the Southern Hemisphere's atmospheric circulation during Dansgaard–Oeschger cycles is lacking. Here we use a high-resolution deuterium-excess record from West Antarctica to show that the latitude of the mean moisture source for Antarctic precipitation changed in phase with abrupt shifts in Northern Hemisphere climate, and significantly before Antarctic temperature change. This provides direct evidence that Southern Hemisphere mid-latitude storm tracks shifted within decades of abrupt changes in the North Atlantic, in parallel with meridional migrations of the intertropical convergence zone. We conclude that both oceanic and atmospheric processes, operating on different timescales, link the hemispheres during abrupt climate change.

Dansgaard–Oeschger (DO) events in the Northern Hemisphere (NH)[1,2] and Antarctic isotope maximum (AIM) events in the Southern Hemisphere (SH) are coupled by variations in meridional oceanic heat transport. The large effective heat capacity of the SH oceans integrates the abrupt changes in oceanic heat transport[3], leading to the muted, out-of-phase character of Antarctic temperature variations[4]. The Antarctic temperature response systematically lags abrupt DO transitions by about two centuries, a timescale consistent with oceanic processes[5].

To satisfy the top-of-atmosphere energy budget, interhemispheric oceanic heat flux anomalies must be accommodated by opposing changes in atmospheric heat transport[6] or changes in local radiative processes. While atmospheric models do not necessarily agree on the relative roles of these mechanisms, some responses are robust, such as migration of the Hadley circulation and intertropical convergence zone (ITCZ) toward the warmer hemisphere[6,7]. Recent studies suggest that ITCZ migration can influence the position of the SH eddy-driven jet and surface westerlies[8,9]. The SH mid-latitude westerlies are a key component of the global climate, transporting heat and momentum toward the pole and influencing Southern Ocean wind-driven upwelling[10] and ocean–atmospheric CO_2 exchange[11]. Evidence for abrupt changes in tropical circulation and precipitation, synchronous with NH DO events, comes from sediment cores[12–14] and speleothem records[15]. In contrast, evidence for corresponding millennial-scale changes in the dynamics or meridional position of the SH westerlies is wanting[16].

New constraints from ice core records

Here, we use deuterium-excess data from the West Antarctic ice sheet (WAIS) Divide ice core (WDC) to constrain changes in SH atmospheric circulation during DO events. Deuterium excess ($d_{excess} = \delta D - 8 \times \delta^{18}O$) of vapour quantifies kinetic fractionation processes and is sensitive to sea surface temperature (SST) and relative humidity at the site of evaporation[17]. Variability in the SST-normalized humidity, the critical moisture source condition driving kinetic fractionation[17], is probably dominated by changes in SST on millennial timescales, although relative humidity may also be important (Supplementary Information). The d_{excess} is also directly affected by SST through the temperature dependence of fractionation at evaporation[17]. The d_{excess} of polar precipitation reflects the weighted-mean evaporative conditions of moisture sources, whose spatial distribution is sensitive to changes in atmospheric circulation.

Interpretation of Antarctic d_{excess} records has been hampered by the absence of a coherent signal among Antarctic cores[18,19] (Fig. 1a). We find that the lack of coherence is largely an artefact of the linear definition of d_{excess}. Equilibrium fractionation alone leads to a nonlinear relationship between δD and $\delta^{18}O$ (ref. 20) that is most evident at the very depleted values in East Antarctic precipitation (Supplementary Information). We instead use a logarithmic definition[21] for the parameter, $d_{ln} = \ln(\delta D + 1) - (8.47 \ln(\delta^{18}O + 1) - 2.85 \times 10^{-2}(\ln(\delta^{18}O + 1))^2)$, which better represents the underlying distillation physics and is a more faithful proxy for moisture source variability (Supplementary Information).

[1]Department of Earth and Space Sciences, University of Washington, Seattle, Washington 98195-1310, USA. [2]Department of Atmospheric Sciences, University of Washington, Seattle, Washington 98195-1640, USA. [3]College of Earth, Oceanic and Atmospheric Sciences, Oregon State University, Corvallis, Oregon 97331, USA. [4]Centre for Ice and Climate, University of Copenhagen, Copenhagen DKK-2100, Denmark. [5]Department of Geography, University of California, Santa Barbara, California 93016, USA. [6]Institute of Arctic and Alpine Research, University of Colorado, Boulder, Colorado 80309, USA. [7]Department of Geosciences, Pennsylvania State University, University Park, Pennsylvania 16802, USA. *e-mail: marklebr@uw.edu

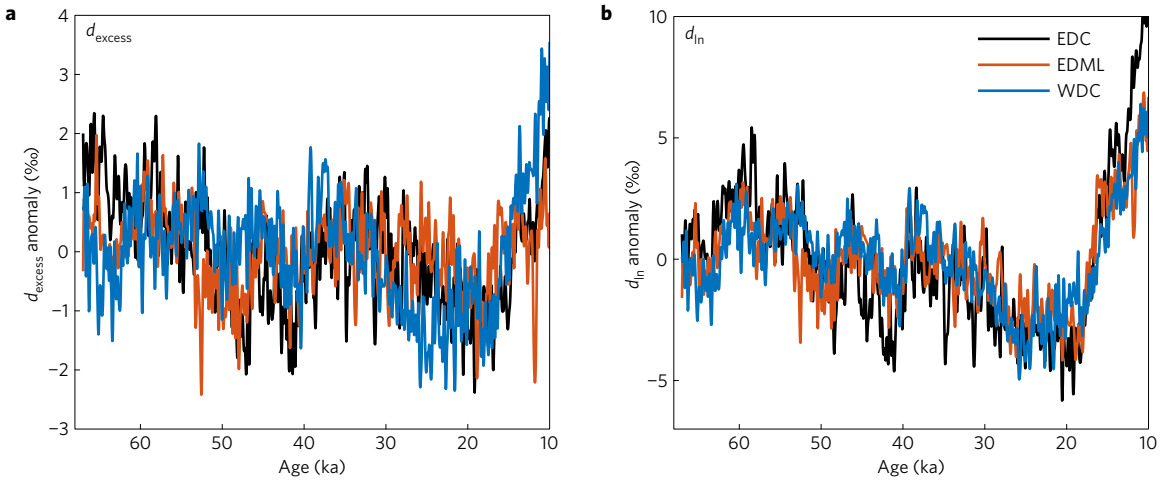

Figure 1 | Comparison of deuterium-excess definitions for multiple ice cores. Anomalies are the deviation from the 10 ka to 67 ka mean. A low-pass, fourth-order Butterworth filter with a 1 cycle per 300 yr cutoff frequency has been applied to all curves for visual clarity. **a**, Time series of d_{excess} for WDC (blue), EDML (red) and EDC (black). Correlation coefficient for WDC–EDML: 0.13; WDC–EDC: 0.25; EDC–EDML: 0.31. **b**, As above but for the d_{ln} definition. Correlation coefficient for WDC–EDML: 0.62; WDC–EDC: 0.68 ; EDC–EDML: 0.74.

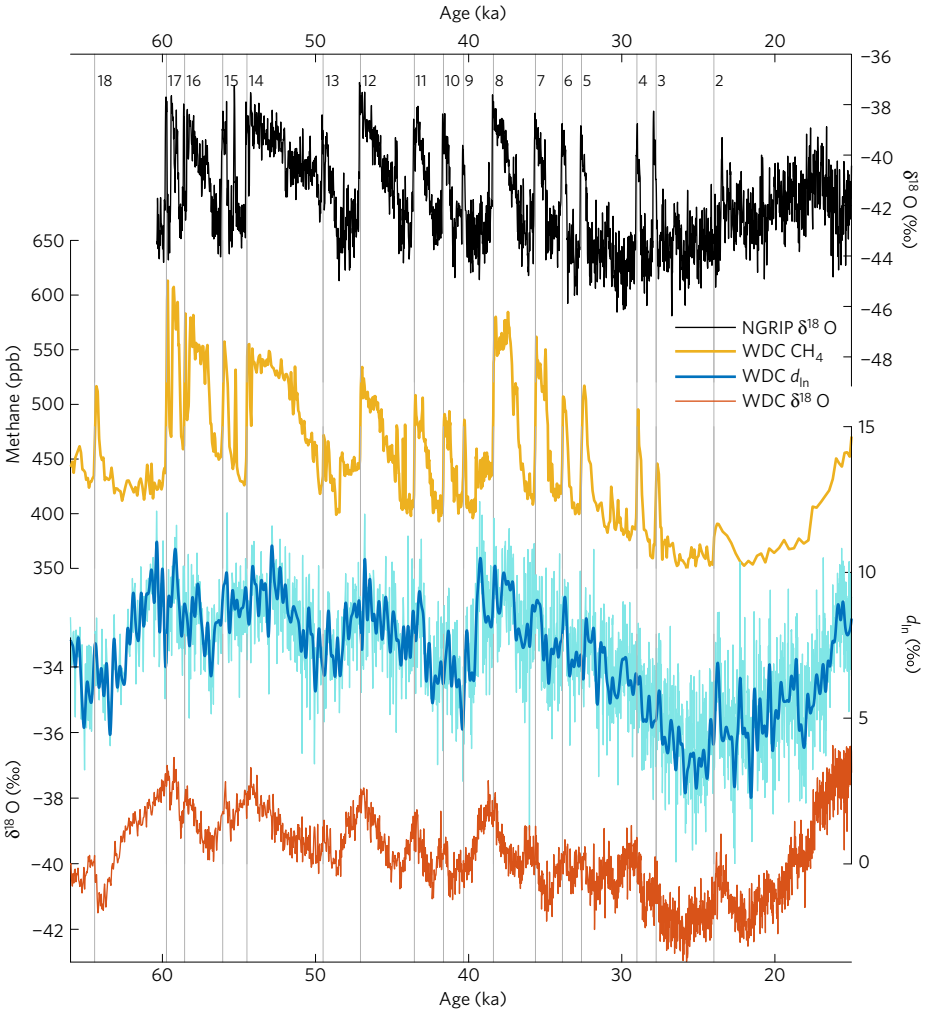

Figure 2 | Proxy records from the last glacial period. Greenland $\delta^{18}O$ record from NGRIP on 1.0063 × GICC05 chronology[23] (black). WDC CH_4 (gold), WDC $\delta^{18}O$ (red), WDC d_{ln} (cyan) and filtered d_{ln} (blue) on the WD2014 chronology[23]. High-frequency variability (>1 cycle per 300 yr) removed from filtered d_{ln} by a low-pass Butterworth filter for visual clarity. DO events are numbered and the timings of their midpoints are indicated by vertical grey lines.

While conventionally defined East Antarctic d_{excess} records from EPICA Dronning Maud Land (EDML) and EPICA Dome C (EDC)[18] show no significant coherence with WDC d_{excess} at any timescale, the logarithmically defined d_{ln} records from all three cores are significantly coherent with each other at all periods greater than 3,000 years (Fig. 1). Degradation of coherence at

shorter timescales is expected due to chronological uncertainties. Equilibrium fractionation biases, rather than spatial asymmetries in the climate, clearly dominate the differences among linearly defined d_{excess} records, while the d_{ln} records reveal a coherent signal.

Analysis of millennial-scale variability

We compare high-resolution WDC d_{ln} with WDC atmospheric methane (CH_4) concentrations and with WDC $\delta^{18}O$, a proxy for site temperature (Fig. 2). Global CH_4 variations are in phase with Greenland temperature within a few decades[22] and are thought to reflect changes in tropical precipitation and temperature associated with the north–south migration of the ITCZ during DO events[15,22], thus serving as an indicator for shifts in tropical circulation[5]. We compare these records (Fig. 2) to establish the phasing between changes in Antarctic moisture sources and SH, tropical and NH climate during DO events. The WDC records are uniquely suited for this purpose owing to the small and well-constrained gas age–ice age difference (Δage)[5]. The Δage is calculated continuously through the core and is 351 $\pm$ 73 years (2σ) at 40 thousand years ago (ka), a value representative of the last glacial period[23].

The d_{ln} records from WDC, EDC and EDML on average show gradual millennial-scale variability in phase with the AIM events seen in Antarctic $\delta^{18}O$ records (Fig. 1b). However, WDC d_{ln} also exhibits variability that tracks CH_4 through the DO cycles (Fig. 2). Since the subjective appearance of individual events may be confounded by noise inherent to the proxies and the physical systems they record, we use objective techniques to quantify these relationships across all events.

We first evaluate the WDC data using a multitaper coherency and phase analysis (Methods). The WDC $\delta^{18}O$, d_{ln} and CH_4 records are all significantly coherent with one another across millennial timescales. The WDC $\delta^{18}O$ and CH_4 records have a phase relationship of ~90° at millennial timescales, reflecting integration of the NH DO events by SH climate, and a ~200 year lag of WDC $\delta^{18}O$ behind CH_4. The millennial variability in d_{ln} is coherent with both $\delta^{18}O$ and CH_4 at phase angles between 0° (in phase) and 90°, consistent with a signal that contains both DO and AIM modes of variability. Indeed, a simple linear combination of the WDC $\delta^{18}O$ and CH_4 signals is coherent and in phase with WDC d_{ln} at all timescales and is a significantly better predictor of d_{ln} than either $\delta^{18}O$ or CH_4 individually. Together, the CH_4 and $\delta^{18}O$ signals explain 62% of all variance in d_{ln} and more than 85% of the variance at relevant timescales (those longer than 500 years).

Next, to investigate the character of DO-like variability recorded in WDC d_{ln}, we construct composites of the d_{ln} record during abrupt NH warming and cooling events. We use the stacking procedure described in ref. 5, in which all individual events in all WDC proxies are aligned at the midpoints of the abrupt CH_4 transitions and averaged to obtain a composite event; this allows direct comparison with DO events from the North Greenland Ice Core Project (NGRIP) $\delta^{18}O$ record from Greenland[24] and reduces the noise inherent to any single event. We use objective algorithms[25] to determine the timing of significant change in the WDC d_{ln}, NGRIP $\delta^{18}O$, WDC CH_4 and WDC $\delta^{18}O$ composites (Methods).

We find that the composite d_{ln} response at the timing of DO warming and cooling events is step-like and occurs within decades (synchronous within uncertainty) of NH (NGRIP $\delta^{18}O$) and tropical (CH_4) step changes. The initial change points in the DO warming event stacks of NGRIP $\delta^{18}O$, WDC CH_4, and WDC d_{ln} occur at -27 ± 5 years (1σ), 18 ± 14 years, and 45 ± 83 years, respectively, with the timing given relative to the midpoint of the NGRIP $\delta^{18}O$ abrupt changes (Fig. 3; see Methods for a full description of uncertainties). For DO cooling events, the initial change points in the NGRIP $\delta^{18}O$, WDC CH4, and WDC d_{ln} stacks occur at -36 ± 7 years, -24 ± 14 years, and -27 ± 70 years, respectively. In both cases, the change point in WDC d_{ln} occurs significantly before the change point in WDC $\delta^{18}O$; d_{ln} leads $\delta^{18}O$ by 173 ± 79 years for DO warming, and 235 ± 64 years for DO cooling.

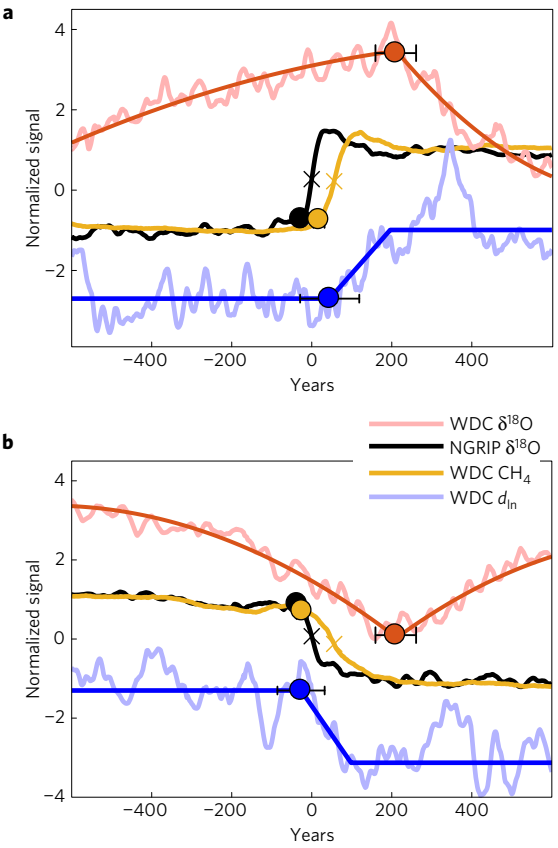

Figure 3 | DO event compositing analysis. a,b, DO warming (**a**) and cooling (**b**) stacks for NGRIP $\delta^{18}O$ (black), WDC CH_4 (gold), WDC $\delta^{18}O$ (red), and WDC d_{ln} (blue) with fits (bold; see Methods). WDC events are aligned on the midpoint of the abrupt WDC CH_4 transition (yellow cross), which is set to lag the Greenland $\delta^{18}O$ midpoint (black cross) by 56 years (Methods). The timings of initial change points in all stacks (dots) are shown with respect to the Greenland $\delta^{18}O$ midpoint, with 2σ uncertainty bars that reflect the full combination of age-scale, stacking, and change point detection uncertainties (see Methods).

Global teleconnections

To elucidate the sources of WDC d_{ln} variability, we review the processes thought to communicate climate signals between the hemispheres during DO and AIM events. First, variations in northward heat transport by the ocean warm one hemisphere at the expense of the other[4]. The surface temperature response to heating changes in the North Atlantic is abrupt, driving the DO signal. Second, the Southern Ocean integrates the changes in northward heat transport, resulting in the gradual, out-of-phase variations in Southern Ocean and Antarctic temperature[3]: the AIM signal. There is a discrete ~200 year lag between the abrupt DO events and the transition between warming and cooling of the AIM events, probably reflecting an oceanic transport timescale[5]. Third, the thermal asymmetry between the hemispheres drives a fast ($\leq$decadal) atmospheric response in which the ITCZ migrates toward the warmer hemisphere[6]. Fourth, a related atmospheric teleconnection links migration of the ITCZ to shifts in the meridional position of the storm tracks in the Southern Hemisphere[8]. This teleconnection would link the position of the Southern winds to events in the tropics and high NH latitudes on short atmospheric timescales, despite gradual and lagged changes in mean SH temperatures.

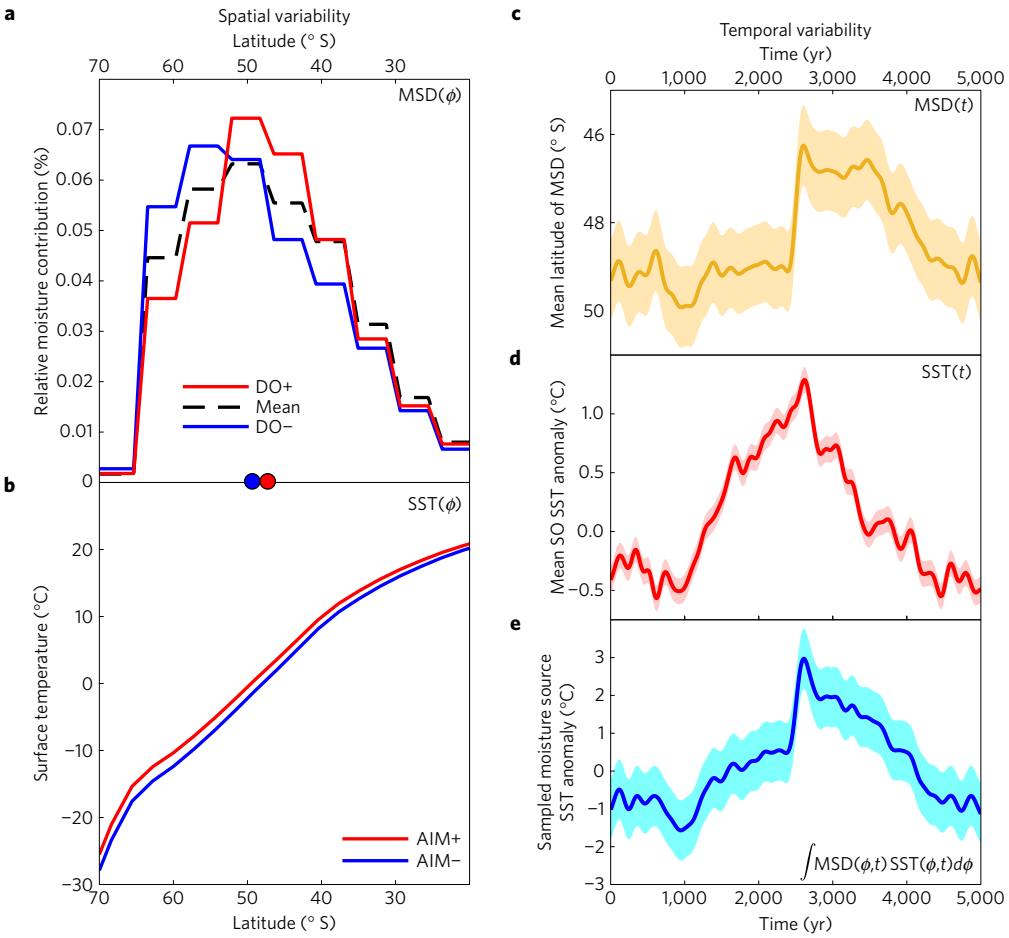

Figure 4 | Schematic of spatial and temporal variability in moisture sources during an idealized DO/AIM cycle. a, The modelled mean moisture source distribution (MSD(ϕ), black dashed) for WDC (Supplementary Information) is represented as a histogram of the latitude of initial evaporation. Modelled MSDs associated with strongly northward (red) and southward (blue) shifts in the position of the Southern Hemisphere winds are associated with DO warming (+) and cooling (−) events. The weighted-mean latitudes of the displaced MSDs are shown as dots along the bottom axis. **b**, Idealized spatial patterns of surface temperature during warm (AIM+) and cold (AIM-) phases of AIM events, showing the strong meridional gradient of SST(ϕ). **c**–**e**, Schematics of the temporal evolution of the mean MSD latitude for WDC (**c**), the mean surface temperature anomaly in the Southern Ocean (**d**) and the mean sampled moisture source temperature resulting from the superposition of **c** and **d** (**e**). Shaded bands reflect the expected levels of internal noise for each variable. Details of the schematics are described in the Supplementary Information.

A simple framework reconciles the combined AIM-like and DO-like signals in WDC d_{ln} in light of the above processes. Variability in d_{ln} represents the superposition of two primary mechanisms: changes in moisture source conditions at fixed locations and changes in the spatial distribution of moisture sources for an ice core site. In short, the spatial–temporal pattern of SSTs is weighted by the spatial–temporal pattern of the moisture source distribution (MSD) (Fig. 4). In the zonal mean, and given a linear SST–d_{ln} scaling, $d_{ln}(t) \propto \int \mathrm{MSD}(\phi,t)\mathrm{SST}(\phi,t)\,\mathrm{d}\phi + \nu$, where ϕ and t denote dependence on latitude and time, and ν denotes other sources of variability.

Owing to the first and second processes above, changes in Southern Ocean heat content are thought to drive the gradual Antarctic surface temperature variability of AIM events[3] via changes in Southern Ocean SSTs[26]. Southern Hemisphere SST(t) within the moisture source thus drives AIM-like variations in Antarctic d_{ln} (Fig. 4), accounting for the gradual variability observed in the WDC, EDML and EDC records.

A large equator-to-pole gradient dominates the spatial pattern of SST(ϕ) in the SH (Fig. 4). Meridional shifts in the mean location of the moisture source, toward more equatorward or more poleward surface waters, change the sampled mean SST at evaporation due to the steep underlying gradient. Changes in MSD(ϕ) can therefore change the d_{ln} at an ice core site, independent of any temporal variability in the SSTs themselves. General circulation model simulations (Supplementary Information) show that the latitudinal distribution of moisture sources for WAIS Divide change in parallel with the meridional position of the SH westerly winds and ITCZ, changing the sampled SST and d_{ln} of precipitation (Fig. 4).

The atmospheric teleconnections predicted during abrupt climate change, the third and fourth processes described above, are recorded in the WDC d_{ln} shifts that occur synchronously with NH DO events (Fig. 3). An abrupt DO event shifts the position of the tropical Hadley cell, causing a parallel shift in the SH surface westerlies and storm tracks in the Pacific sector[8,9], changing the moisture origin for West Antarctica. Thus, abrupt changes in moisture source location superimposed on gradual changes in moisture source temperatures lead to the observed combination of DO-like and AIM-like variability in WDC d_{ln} (Fig. 4).

We calculate the scaling of d_{ln} variations to source-region SSTs in a simple distillation model and an isotope-enabled general circulation model (Supplementary Information). SH SST changes on the order of 1–2 K, in phase with the AIM events, and meridional MSD shifts of 1°–2° latitude, in phase with DO events, together account for the bulk of observed variability in WDC d_{ln} (Fig. 4). Southern Ocean SST changes of this magnitude are in line

with independent estimates from sediment cores[26]. The required MSD shifts are comparable to those associated with westerly wind displacement at the 1–1.5σ level of interannual variability, amounting to 15–20% anomalies in surface winds (Supplementary Information). Storm track shifts of this magnitude during DO events are in good agreement with estimates of ITCZ displacement from proxy data[27] and the modelled relationship between the ITCZ and the SH circulation[8]. Our results are supported by previous modelling showing anti-correlation between Antarctic deuterium excess and the Southern Annular Mode index[28].

Did the atmospheric circulation shift zonally across the entire SH during DO events[8], or were changes limited to the Pacific sector (ref. 9)? East Antarctic records may inform this question. EDC d_{ln} shows variability during DO 8 and 12 out of phase with local $\delta^{18}O$ (ref. 19) and similar to WDC (Supplementary Information). However, unambiguous characterization of the variability in East Antarctic d_{ln} records is currently hampered by uncertainties in East Antarctica Δage, and the lack of synchronization between the WD2014[23] and AICC2012[29] age scales.

Conclusions

Our new data from WDC demonstrate the importance of both oceanic and atmospheric teleconnections linking the climate of the Northern and Southern hemispheres on millennial timescales. SH SSTs followed the temporal signature of the AIM events, driven by oceanic heat transport changes. SH winds shifted in phase with the NH DO events, reflecting coupled changes in global atmospheric circulation. These atmospheric teleconnections were rapid, shifting the position of the moisture source locations for WDC (recorded in d_{ln}) within decades of NH DO events and about two centuries before significant Antarctic temperature change (recorded in $\delta^{18}O$). Our findings complement evidence for atmospheric-circulation-imposed variability in Greenland deuterium excess[30]. Atmospheric dynamics link the tropical Hadley circulation to the mid-latitude storm tracks in both hemispheres. A global 'atmospheric seesaw' is superimposed on the classic oceanic bipolar seesaw, and may be important to the dynamics of millennial climate change.

Methods

Methods, including statements of data availability and any associated accession codes and references, are available in the online version of this paper.

Received 28 May 2016; accepted 1 November 2016; published online 12 December 2016

References

1. Dansgaard, W. *et al*. A new Greenland deep ice core. *Science* **218,** 1273–1277 (1982).
2. Sachs, J. P. & Lehman, S. J. Subtropical North Atlantic temperatures 60,000 to 30,000 years ago. *Science* **286,** 756–759 (1999).
3. Stocker, T. F. & Johnsen, S. J. A minimum thermodynamic model for the bipolar seesaw. *Paleoceanography* **18,** 1087 (2003).
4. Blunier, T. *et al*. Asynchrony of Antarctic and Greenland climate change during the last glacial period. *Nature* **394,** 739–743 (1998).
5. WAIS Divide Project Members. Precise interpolar phasing of abrupt climate change during the last ice age. *Nature* **520,** 661–665 (2015).
6. Kang, S. M., Frierson, D. M. W. & Held, I. M. The tropical response to extratropical thermal forcing in an idealized GCM: the importance of radiative feedbacks and convective parameterization. *J. Atmos. Sci.* **66,** 2812–2827 (2009).
7. Broccoli, A. J., Dahl, K. A. & Stouffer, R. J. Response of the ITCZ to Northern Hemisphere cooling. *Geophys. Res. Lett.* **33,** L01702 (2006).
8. Ceppi, P., Hwang, Y.-T., Liu, X., Frierson, D. M. W. & Hartmann, D. L. The relationship between the ITCZ and the Southern Hemispheric eddy-driven jet. *J. Geophys. Res.* **118,** 5136–5146 (2013).
9. Chiang, J. C. H., Lee, S.-Y., Putnam, A. E. & Wang, X. South Pacific Split Jet, ITCZ shifts, and atmospheric North–South linkages during abrupt climate changes of the last glacial period. *Earth Planet. Sci. Lett.* **406,** 233–246 (2014).
10. Marshall, J. & Speer, K. Closure of the meridional overturning circulation through Southern Ocean upwelling. *Nat. Geosci.* **5,** 171–180 (2012).
11. Anderson, R. F. *et al*. Wind-driven upwelling in the Southern Ocean and the deglacial rise in atmospheric CO_2. *Science* **323,** 1443–1448 (2009).
12. Deplazes, G. *et al*. Links between tropical rainfall and North Atlantic climate during the last glacial period. *Nat. Geosci.* **6,** 213–217 (2013).
13. Peterson, L. C., Haug, G. H., Hughen, K. A. & Röhl, U. Rapid changes in the hydrologic cycle of the tropical Atlantic during the last glacial. *Science* **290,** 1947–1951 (2000).
14. Pedro, J. B. *et al*. The spatial extent and dynamics of the Antarctic cold reversal. *Nat. Geosci.* **9,** 51–55 (2016).
15. Wang, X. *et al*. Interhemispheric anti-phasing of rainfall during the last glacial period. *Quat. Sci. Rev.* **25,** 3391–3403 (2006).
16. Kohfeld, K. E. *et al*. Southern Hemisphere westerly wind changes during the Last glacial maximum: paleo-data synthesis. *Quat. Sci. Rev.* **68,** 76–95 (2013).
17. Merlivat, L. & Jouzel, J. Global climatic interpretation of the deuterium-oxygen 18 relationship for precipitation. *J. Geophys. Res.* **84,** 5029–5033 (1979).
18. Stenni, B. *et al*. The deuterium excess records of EPICA Dome C and Dronning Maud Land ice cores (East Antarctica). *Quat. Sci. Rev.* **29,** 146–159 (2010).
19. Buiron, D. *et al*. Regional imprints of millennial variability during the MIS 3 period around Antarctica. *Quat. Sci. Rev.* **48,** 99–112 (2012).
20. Craig, H. Isotopic variations in meteoric waters. *Science* (1961).
21. Uemura, R. *et al*. Ranges of moisture-source temperature estimated from Antarctic ice cores stable isotope records over glacial–interglacial cycles. *Clim. Past* **8,** 1109–1125 (2012).
22. Baumgartner, M. *et al*. NGRIP CH_4 concentration from 120 to 10 kyr before present and its relation to a $\delta^{15}N$ temperature reconstruction from the same ice core. *Clim. Past* **10,** 903–920 (2014).
23. Buizert, C. *et al*. The WAIS divide deep ice core WD2014 chronology; Part 1: Methane synchronization (68–31 ka BP) and the gas age–ice age difference. *Clim. Past* **11,** 153–173 (2015).
24. North Greenland Ice Core Project Members. High-resolution record of Northern Hemisphere climate extending into the last interglacial period. *Nature* **431,** 147–151 (2004).
25. Mudelsee, M. Ramp function regression: a tool for quantifying climate transitions. *Comput. Geosci.* **26,** 293–307 (2000).
26. Barrows, T. T., Juggins, S., De Deckker, P., Calvo, E. & Pelejero, C. Long-term sea surface temperature and climate change in the Australian–New Zealand region. *Paleoceanography* **22,** PA2215 (2007).
27. Wang, X. *et al*. Wet periods in northeastern Brazil over the past 210 kyr linked to distant climate anomalies. *Nature* **432,** 740–743 (2004).
28. Schmidt, G. A., LeGrande, A. N. & Hoffmann, G. Water isotope expressions of intrinsic and forced variability in a coupled ocean-atmosphere model. *J. Geophys. Res.* **112,** D10103 (2007).
29. Bazin, L. *et al*. An optimized multi-proxy, multi-site Antarctic ice and gas orbital chronology (AICC2012): 120–800 ka. *Clim. Past* **9,** 1715–1731 (2013).
30. Masson-Delmotte, V. GRIP deuterium excess reveals rapid and orbital-scale changes in Greenland moisture origin. *Science* **309,** 118–121 (2005).

Acknowledgements

We thank A. J. Schauer and P. D. Neff for assistance with the measurements, E. J. Brook, V. Gkinis and H. C. Steen-Larsen for insightful discussions, and B. Stenni for sharing data. We acknowledge grants from the US National Science Foundation Division of Polar Programs (0537930, 1043092 to E.J.S.; 0537593, 1043167 to J.W.C.W.; 0538538, 1043500 to T.S.; 0944197 to T.J.F.; 1043518 to E. J. Brook; and 1341497 to C.M.B.). We acknowledge grants from NOAA Climate and Global Change postdoctoral fellowship program, administered by the University Corporation for Atmospheric Research (to C.B.); support from the Joint Institute for the Study of the Atmosphere and Ocean (JISAO Contribution no. 2462) and from a Marie Curie International Incoming Fellowship (to J.B.P.); NASA National Earth and Space Sciences Fellowship (to T.J.F.); and ARCS Foundation scholarship (to B.R.M.).

Author contributions

B.R.M. and E.J.S. wrote the paper and conducted data analysis with assistance from C.B. and J.B.P. Q.D. and C.M.B. provided climate model output. B.R.M., E.J.S. and S.W.S. produced the water-isotope data with T.R.J. and J.W.C.W. T.S. provided the CH_4 data. All authors contributed to the manuscript.

Additional information

Supplementary information is available in the online version of the paper. Reprints and permissions information is available online at www.nature.com/reprints. Correspondence and requests for materials should be addressed to B.R.M.

Competing financial interests

The authors declare no competing financial interests.

Methods

Data. Water $^{18}O/^{16}O$ and $^{2}H/^{1}H$ composition (expressed as $\delta^{18}O$ and δD, respectively) were measured at IsoLab, University of Washington, Seattle, Washington, USA. Measurement techniques are described in refs 31,32. Measurements were made at 0.5 m depth averaged resolution, using laser spectroscopy (Picarro L2120-*i* analyzer). Data are reported relative to the VSMOW (Vienna Standard Mean Ocean Water) standard, and normalized to SLAP (Standard Light Antarctic Precipitation, $\delta^{18}O = -55.5‰$, $\delta D = -428‰$ relative to VSMOW). Measurement resolution is generally better than 40 years per sample for the 67 kyr record, with a mean temporal resolution of 17.2 years per sample between 10–67 ka. Measurement uncertainties are better than 0.08‰ for $\delta^{18}O$ and 0.8‰ for δD.

Atmospheric methane concentrations were measured on discrete samples at Pennsylvania State University (0–67 ka, 0.5–2 m resolution). Air was extracted from ~50 g ice samples using a melt–refreeze technique, and analysed on a gas chromatograph with a flame-ionization detector. Corrections for gas solubility, blank and gravitational enrichment are described in ref. 32.

Dansgaard–Oeschger event compositing. The stacking procedure used in this study is identical to that used in ref. 5. The reader is referred to that study for a complete description of the method and its uncertainties. We summarize and describe additions here. The midpoint of each abrupt DO transition in NGRIP $\delta^{18}O$ and WDC CH_4 is identified following ref. 23 and used as a tie point for each DO/AIM event. A time vector, t, is defined from −1,200 years to 1,200 years with 1-year spacing. For each DO/AIM event, the NGRIP $\delta^{18}O$ and WDC CH_4, $\delta^{18}O$ and d_{ln} data are linearly interpolated onto time vector t. The midpoints of each DO transition in NGRIP $\delta^{18}O$ are fixed to time $t = 0$ years, and WDC CH_4 midpoint at time $t = 56$ years, which is the average lag of atmospheric CH_4 behind Greenland $\delta^{18}O$ as identified by ref. 22. The relative timing of the WDC isotope records to WDC CH_4 are linked by the small and relatively well-constrained gas age–ice age difference (Δage) of the WAIS Divide core[23]. All DO/AIM events are then stacked and averaged creating a composite DO/AIM event for each proxy. Our results are robust to the set of events composited, for example, the dropping of random events from the composite and the exclusion of large or small events.

Before stacking, we filter the WDC d_{ln} record to reduce noise. WDC d_{ln} has power at millennial frequencies comparable to that in WDC CH_4 and $\delta^{18}O$ as well as high-frequency noise unrelated to the millennial variability of interest here. We wish to reduce high-frequency noise due to measurement, which is normally distributed in the depth domain. We apply a 1-2-1 filter to the raw d_{ln} data on the measured depth scale, which is a tapered weighting function similar to a 3-point moving average but twice the weight is given to the central point. Its response function has a relatively sharp frequency cutoff and is never negative (unlike moving averages); thus, no phase shifting of the data occurs. Below, we assess the influence of this light filtering on change point detection.

Breakpoint determination and uncertainties. The stacking procedure demonstrates the average response of d_{ln} to abrupt DO transitions and quantifies lags. To objectively identify change points in the composites we use the RAMPFIT[25] and BREAKFIT[33] algorithms. The use of a modified BREAKFIT change point detection on the WDC $\delta^{18}O$ is discussed extensively in ref. 5. RAMPFIT is better suited to this study than BREAKFIT, due to the ramp-like shape of the d_{ln}, CH_4 and NGRIP $\delta^{18}O$ composites, although results from both algorithms are comparable (discussed below) and do not affect the conclusions of this study. RAMPFIT has been used previously to detect abrupt change in deuterium-excess records[34]. The RAMPFIT algorithm fits a ramp function, consisting of three linear sections and two break points (t_1 and t_2), to the data in a least-squares sense. We let the algorithm search for the initial breakpoint, t_1, within the bounds −200 to 200 years, and the second break point, t_2, within the bounds −100 to 350 years on the WDC d_{ln} composite (recall that the midpoint of the DO transition in NGRIP $\delta^{18}O$ is defined at $t = 0$ years, and the WDC CH_4 midpoint at time $t = 56$ years). The algorithm finds the best-fit ramp function defined by the mean of the 'before' and 'after' line segments, the duration of the ramp, and the timing of t_1 and t_2. The algorithm uses a Monte Carlo moving block bootstrap (MBB) technique[33] to address uncertainty in the identification of the breakpoints. We report the mean and standard deviation of the initial breakpoint, t_1, as the timing of initial d_{ln} change.

We investigate the influence of the choice of smoothing filter applied to the raw d_{ln} record prior to the stacking procedure. We evaluate three different types of smoothing: a 1-2-1 filter; a 1-1-1 filter, that is, a 3-point symmetrically applied moving average; no filtering. The results are summarized in Supplementary Table 1 and shown in Supplementary Fig. 1. The choice of filter slightly influences the mean timing of the change points as detected by RAMPFIT, but in all cases the initial change points, t_1, are in agreement within uncertainty. Further, in all cases t_1 is synchronous with the initiation of abrupt change in WDC CH_4 within uncertainty.

In the stacking procedure, the individual events in all proxies from WDC are aligned at the midpoint of the WDC CH_4 transitions. However, the exact alignment of events is subject to uncertainty. We perform a Monte Carlo sensitivity analysis (1,000 realizations) in which random perturbations in timing are applied to the individual d_{ln} events that make up the d_{ln} stacks, following ref. 5. These timing uncertainties are discussed in detail in ref. 5. We use the non-systematic errors from that study, which include uncertainty in determining the midpoint of the abrupt shifts in both NGRIP $\delta^{18}O$ and WDC CH_4; variability in the stated 56 yr lag of WDC CH_4 behind shifts in NGRIP $\delta^{18}O$; and non-systematic errors related to the age-scale construction[5,23]. Random timing errors within the stated uncertainties of ref. 5 are applied to the unfiltered, individual d_{ln} events. The events are stacked as above and 1,000 realizations are averaged. The resulting composite has a very high signal-to-noise ratio, as uncorrelated variations are heavily reduced. The RAMPFIT routine was performed on the resulting composite d_{ln} response, yielding an initial d_{ln} breakpoint at $t_1 = 51 \pm 33$ yr and $t_1 = -35 \pm 36$ yr for the DO warming and cooling phases, respectively. Our results are thus robust to timescale uncertainties.

An important source of uncertainty in the timing of the breakpoint relative to the abrupt DO transitions is the gas age–ice age difference (Δage). An extensive analysis of this uncertainty is presented in ref. 5. As the $\delta^{18}O$ and d_{ln} are measured on the same ice, the 2σ uncertainty bound of 69 years due to Δage, found by ref. 5, is applicable to the d_{ln} composite as well. However, the relative timings of breakpoints in the WDC $\delta^{18}O$ and d_{ln} stacks are not subject to any uncertainty associated with Δage, since they are measured on the same ice samples. Thus, our claim that the breakpoint in the d_{ln} stack occurs significantly before the $\delta^{18}O$ breakpoint relies solely on the identification of the breakpoint, and not Δage uncertainties. We find that the d_{ln} change point occurs significantly before that in $\delta^{18}O$ by an amount of 173 ± 79 yr for the DO warming, and by 235 ± 64 yr for DO cooling.

As a further test of the robustness of our change point detection, we apply the BREAKFIT algorithm to the d_{ln} composite of DO warming events (instead of the RAMPFIT routine used above). The d_{ln} breakpoint as found by the BREAKFIT method ($t = 23 \pm 38$ yr for raw data, and $t = 38.4 \pm 25.4$ yr for filtered data) is in good agreement with results from the RAMPFIT method.

Summary of change point uncertainties. Here we briefly synthesize the above sensitivity studies and uncertainties in the timing of the d_{ln} breakpoints. For the phasing of WDC d_{ln} breakpoints to NGRIP $\delta^{18}O$ we consider: the RAMPFIT MBB uncertainty, ±74 yr (1σ) for DO warming and ±59 yr for DO cooling; the Δage uncertainty[5], ±69 yr (2σ); the systematic uncertainty in the NGRIP $\delta^{18}O$-WDC CH_4 phasing from ref. 5, ±27 yr (2σ). Adding all uncertainties in quadrature yields ± 83 yr (1σ) for DO warming events, and ±70 yr (1σ) for DO cooling events, as reported in the main text.

We can similarly quantify the uncertainty in the WDC CH_4, and NGRIP $\delta^{18}O$ initial break points, as found by the RAMPFIT analysis. In the case of WDC CH_4, we consider the RAMPFIT MBB uncertainty, ±4 yr (1σ) for DO warming and ±2 yr for DO cooling; and the systematic uncertainty in the NGRIP $\delta^{18}O$-WDC CH_4 phasing, ±27 yr (2σ). Adding all uncertainties in quadrature yields ±14 yr (1σ) for both DO warming and cooling events (rounding uncertainties to the nearest year). For the NGRIP $\delta^{18}O$ change points, we consider only the RAMPFIT MBB uncertainty of ±5 yr (1σ) and ±7 yr, for warming and cooling events, respectively. Note that owing to the much higher signal-to-noise ratio of the NGRIP $\delta^{18}O$ and WDC CH_4 stacks, the MBB uncertainties are much lower than those of WDC d_{ln}.

For the phasing of WDC d_{ln} to WDC $\delta^{18}O$ breakpoints we consider only the RAMPFIT MBB uncertainty for the d_{ln} breakpoint, ±74 yr (1σ) for DO warming and ±59 yr for DO cooling, and the BREAKFIT uncertainty for the $\delta^{18}O$ breakpoint[5], ±50.8 yr (2σ). Adding in quadrature yields phasing uncertainties of ±79 yr (1σ) for DO warming events and ±64 yr (1σ) for DO cooling events.

Frequency domain methods. We use the Thompson multitaper method for coherence and phase estimates, correcting for coherence bias and using a Monte Carlo approach to estimate the 95% confidence limits on the phase estimation (for example, ref. 35). We also use the Thompson multitaper method to estimate spectral power density, employing the MATLAB pmtm.m routine with an improved confidence limit estimation that correctly accounts for the degrees of freedom as implemented by P. Huybers (http://www.people.fas.harvard.edu/~phuybers/Mfiles). We linearly interpolate the data to even time intervals ($\Delta t = 10$ yr spacing) before analysis. We perform the analysis on the records over the interval 10–67 ka, 20–67 ka (excluding the deglaciation), 6–67 ka (including the early Holocene), and for different interpolated time spacing ($\Delta t = 10$, 20, 40 years). These analytical choices do not meaningfully impact the conclusions of this study.

Characterization of millennial frequencies. We characterize the WDC d_{ln}, CH_4 and $\delta^{18}O$ spectra, providing context for interpreting the phase relationship of WDC d_{ln} to the AIM and DO patterns of climate variability. Normalized (z-score over the 10–67 ka period) CH_4 and $\delta^{18}O$ have red power spectra, with increasing power toward lower frequencies through the millennial band; AIM and DO cycles are not

periodic but span a range of timescales from ~500 to 5,000 years. Millennial-scale power in normalized d_{ln} is comparable to that of CH_4 and $\delta^{18}O$. It is important to note that while the $\delta^{18}O$ and CH_4 signals are both expressions of millennial variability in the coupled climate system, they do not have the same power distribution across frequency. Specifically, millennial-band power in WDC $\delta^{18}O$ is weaker than that in CH_4 (or Greenland $\delta^{18}O$). The distribution of millennial power in WDC d_{ln} has similarities to that of both CH_4 and WDC $\delta^{18}O$.

The unique nature of the millennial band is shown clearly in the coherence and phase between WDC CH_4 and $\delta^{18}O$ (Supplementary Fig. 2). The phase relationship transitions from in phase at orbital frequencies, to ~90° out of phase at millennial frequencies (~5 to 1 kyr periods of the DO/AIM cycles). This relationship reflects the integrand–integrator relationship between NH and SH climate: temperature change in the North Atlantic (highly correlated with WDC CH_4) is inversely related to the time rate of change of temperature in the Southern Hemisphere[36]. Any signal is 90° out of phase with its derivative across frequency, and has reduced power compared with the derivative. The smoothly decreasing phase angle between WDC CH_4 and $\delta^{18}O$ at periods below ~2,000 yr is equivalent to the discrete ~200 yr time lag between the Northern and Southern hemispheres during these events[5]. A discrete time lag between two signals, $-\Delta\tau$, is equivalent to a smoothly changing phase angle $\emptyset = -\Delta\tau \times \omega \times 360°$ with frequency ω (ref. 37).

The d_{ln} record is significantly coherent with both CH_4 and $\delta^{18}O$ (Supplementary Fig. 2), but shows a distinct phase relationship: at periods <2.5 kyr, d_{ln} and CH_4 are essentially in phase; at timescales between ~2.5 kyr and 5 kyr, d_{ln} is out of phase with both $\delta^{18}O$ and CH_4, with a phase angle between 0° (in phase) and 90° (quadrature). One should expect d_{ln} to show phase angles between 0° and 90° with $\delta^{18}O$ and CH_4, if its variability were composed of a superposition of two modes of variability, one in phase with $\delta^{18}O$ and the other in phase with CH_4 (which are 90° to each other). Below we show that the relationship of phase angle to frequency observed among the records is expected if d_{ln} represents a combination of the CH_4 and $\delta^{18}O$ modes of variability, given the distribution of power in the CH_4 and $\delta^{18}O$ records.

Sensitivity of phase relationships to chronological uncertainties. We investigate the sensitivity of the coherence analysis to chronological uncertainties in the age model and Δage history arising from the dynamical firn densification model on which they are based[23]. We perform a Monte Carlo sensitivity study in which the coherence and phase between WDC CH_4, $\delta^{18}O$ and d_{ln} are calculated for an ensemble of 10^3 different possible Δage histories that are generated by varying input parameters to the firn densification model[23] within stated uncertainties, as well as four different depth interpolation schemes[38] for a total of 4×10^3 possible WDC chronologies. The mean coherence and phase of the Monte Carlo sensitivity study are shown in Supplementary Fig. 2a,b with $\pm 1\sigma$ of the spread of results (shading). The results demonstrate that the coherence and phase analysis is insensitive to the small chronological uncertainties of the WDC timescale. The 95% confidence intervals on the estimation of the phase relationship between WDC CH_4, $\delta^{18}O$ and d_{ln} calculated by the cmtm.m routine using an iterative method[35] are shown in Supplementary Fig. 2c.

Regression model. WDC d_{ln} variability is related to the variability in both WDC CH_4 and $\delta^{18}O$. We illustrate this explicitly by multiple linear regression of the combined CH_4 and $\delta^{18}O$ signals to WDC d_{ln}, $\langle d_{ln}\rangle = a\langle\delta^{18}O\rangle + b\langle CH_4\rangle$, where $\langle x\rangle$ indicates that time series x has been normalized by its z-score over the interval 10–67 ka. The combined regression model ($a = 0.4589$ and $b = 0.3951$) accounts for 62% of variance of the d_{ln} record at all timescales (Supplementary Fig. 3). The F statistic of the combined model, 4666.3, has a p value within rounding error of zero, indicating that the combined regression model is a significantly better predictor of the d_{ln} record than the $\delta^{18}O$ or CH_4 component alone. Much of the remaining variance in WDC d_{ln} not described by the combined model can be attributed to high-frequency noise in WDC d_{ln}; the linear model explains over 87% of the variance in WDC d_{ln} if high-frequency noise (<1 cycle per 500 yr) is excluded.

We use a Monte Carlo method to test whether the additional variance explained by the combined linear model is significant over that explained by its components alone, accounting for autocorrelation in the time series. We compare the linear regression model, $a\langle\delta^{18}O\rangle + b\langle CH_4\rangle$, against two dummy regression models, $M_1 = a_1\langle\delta^{18}O\rangle + b_1\text{noise}_1$, and $M_2 = a_2\text{noise}_2 + b_2\langle CH_4\rangle$, where $\text{noise}_{1,2}$ are randomly generated AR-1 time series whose mean, standard deviation, and lag-1 autocorrelation match those of the normalized CH_4 and $\delta^{18}O$ time series, respectively. We compare the r^2 of the real linear model with the distribution of r^2 values resulting from 10^3 random iterations of each dummy model. The distributions of r^2 values for M_1 and M_2 have a greatest-likelihood value equal to that of $\delta^{18}O$-only and CH_4-only models, respectively ($r^2 = 0.54$ and $r^2 = 0.51$), with a decreasing but non-zero probability of a higher r^2 value due to noise fitting of the additional random, but autocorrelated, time series. The real linear model's r^2 (0.62) exceeds that of 99.95% and 100% of iterations for M_1 and M_2, respectively. These results demonstrate conclusively that the additional variance in d_{ln} explained by the combined $\delta^{18}O$ and CH_4 variability is significant and not due to noise fitting.

The linear model analysis is consistent with the observed spectral coherency. An arbitrary linear combination of two normalized signals approximately 90° out of phase with each other can result in a signal with any phase relationship to the components. In this case, approximately equal weighting of the components ($a = 0.4589$ and $b = 0.3951$) yields a resulting phase relationship of ~45° between WDC d_{ln} and the components of the model (CH_4 and $\delta^{18}O$). WDC d_{ln} is not precisely 45° to CH_4 and $\delta^{18}O$ at all millennial frequencies. For example, d_{ln} and CH_4 have a phase angle slightly greater than 45° at lower millennial frequencies and closer to 0° at higher millennial frequencies. This reflects differences in the power distribution across millennial frequencies of each proxy and how they combine. The linear model captures the combination of power distribution and phase relationships of d_{ln} to the other proxies: the phase relationship of CH_4 to the linear model is equivalent to the phase relationship of CH_4 to d_{ln}, and likewise for $\delta^{18}O$ to d_{ln} (Supplementary Fig. 4).

Data availability. The data that support the findings of this study are available at http://dx.doi.org/10.17911/S9MW2F.

References

31. Steig, E. J. *et al*. Recent climate and ice-sheet changes in West Antarctica compared with the past 2,000 years. *Nat. Geosci.* **6,** 372–375 (2013).
32. WAIS Divide Project Members. Onset of deglacial warming in West Antarctica driven by local orbital forcing. *Nature* **500,** 440–444 (2013).
33. Mudelsee, M. Break function regression. *Eur. Phys. J. Spec. Top.* **174,** 49–63 (2009).
34. Steffensen, J. P. *et al*. High-resolution Greenland ice core data show abrupt climate change happens in few years. *Science* **321,** 680–684 (2008).
35. Huybers, P. & Denton, G. Antarctic temperature at orbital timescales controlled by local summer duration. *Nat. Geosci.* **1,** 787–792 (2008).
36. Roe, G. H. & Steig, E. J. Characterization of millennial-scale climate variability. *J. Clim.* **17,** 1929–1944 (2004).
37. Wunsch, C. Greenland–Antarctic phase relations and millennial time-scale climate fluctuations in the Greenland ice-cores. *Quat. Sci. Rev.* **22,** 1631–1646 (2003).
38. Fudge, T. J., Waddington, E. D., Conway, H., Lundin, J. M. D. & Taylor, K. Interpolation methods for Antarctic ice-core timescales: application to Byrd, Siple Dome and Law Dome ice cores. *Clim. Past* **10,** 1195–1209 (2014).